Demosaicing With Directional Filtering and *a posteriori* Decision

Daniele Menon, Stefano Andriani, *Student Member, IEEE*, and Giancarlo Calvagno, *Member, IEEE*

***Abstract*—Most digital cameras use a color filter array to capture the colors of the scene. Downsampled versions of the red, green, and blue components are acquired, and an interpolation of the three colors is necessary to reconstruct a full representation of the image. This color interpolation is known as *demosaicing*. The most effective demosaicing techniques proposed in the literature are based on directional filtering and *a posteriori* decision. In this paper, we present a novel approach to this reconstruction method. A refining step is included to further improve the resulting reconstructed image. The proposed approach requires a limited computational cost and gives good performance even when compared to more demanding techniques.**

***Index Terms*—Bayer pattern, color filter array (CFA) interpolation, demosaicing, digital cameras, directional filtering.**

I. Introduction

In a typical digital camera, the colors of the scene are captured by a single CCD or CMOS sensor array, where for each pixel the sensor detects a particular color channel, for example red, green or blue. This kind of sensor is called *Color Filter Array* (CFA). The most popular CFA pattern was introduced by Bayer in [1], and it samples the green band using a quincunx grid, while red and blue are obtained by a rectangular grid, as shown in Fig. 1. In this way, the density of the green samples is twice than that of the red and blue channels. Due to the subsampling of the color components, an interpolation step is required in order to reconstruct a full color representation of the image. This process is called *demosaicing,* and avoiding the introduction of visible artifacts, such as *aliasing* and *zippering,* is desirable.

In literature, many reconstruction algorithms have been presented [2]. The earliest proposed techniques were based on well-known interpolation methods for images, namely nearest-neighbor replication, bilinear interpolation, and cubic spline interpolation, but they were not able to provide good performance.

Better results are achieved by techniques that exploit the interchannel correlation and reconstruct red and blue colors by interpolation of the red-to-green and blue-to-green ratios, as described in [3] and [4].

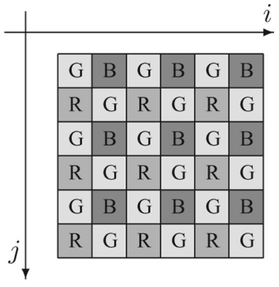

Fig. 1. Bayer pattern.

Other approaches are based on edge-directed interpolation, where the reconstruction is performed in a directional way, so the interpolation is carried out along edges rather than across them. These algorithms use as horizontal and vertical edge-classifiers the gradients [5], [6], the laplacian operator [7], [8], or the jacobian [9], and then they interpolate the green image along the selected direction. Successively they reconstruct the red and blue channels interpolating the color ratios R/G and B/G or the color differences $R-G$, $B-G$.

A class of algorithms such as [10] and [11] propose a weighted sum for the reconstruction of the colors, where every missing sample is estimated by its neighboring pixels and the weights are calculated on the basis of the directions of the edges.

Other more complex approaches are based on different techniques, such as pattern matching [12], pattern recognition [3] or the use of a threshold-based variable number of gradients [13].

Glotzbach *et al.* in [14] propose to use the high-frequency information of the green image to reconstruct the high frequencies of the red and blue components and also to reduce aliasing in the image. Gunturk *et al.* adopt a similar approach in [15] where the high frequencies of the green image are exploited to enhance the red and blue ones. The three channels are reconstructed using an edge-directed interpolation and then each of them is decomposed into four subbands. Afterward, the detail subbands of red and blue are replaced with the detail subbands of the green component.

Another group of methods [16]–[18] proposes a minimum mean-square error (MMSE) solution and discusses ways to reduce the computational complexity.

A very interesting technique employs the reconstruction of two full color images, obtained by interpolation along horizontal and vertical direction, respectively. This leads to two estimation candidates for each pixel and the decision for the best one is made *a posteriori.* In [19], this decision is performed exploiting the local homogeneity of the image, as measured in

Manuscript received October 17, 2005; revised June 14, 2006. This work was supported in part by the 6th Framework Programme IST-MetaCamera Project 2003-506969. The associate editor coordinating the review of this manuscript and approving it for publication was Dr. Luca Lucchese.

The authors are with the Department of Information Engineering, University of Padova, 35131 Padova, Italy.

Color versions of one or more of the figures in this paper are available online at http://ieeexplore.ieee.org.

Digital Object Identifier 10.1109/TIP.2006.884928

1057-7149/$25.00 © 2006 IEEE

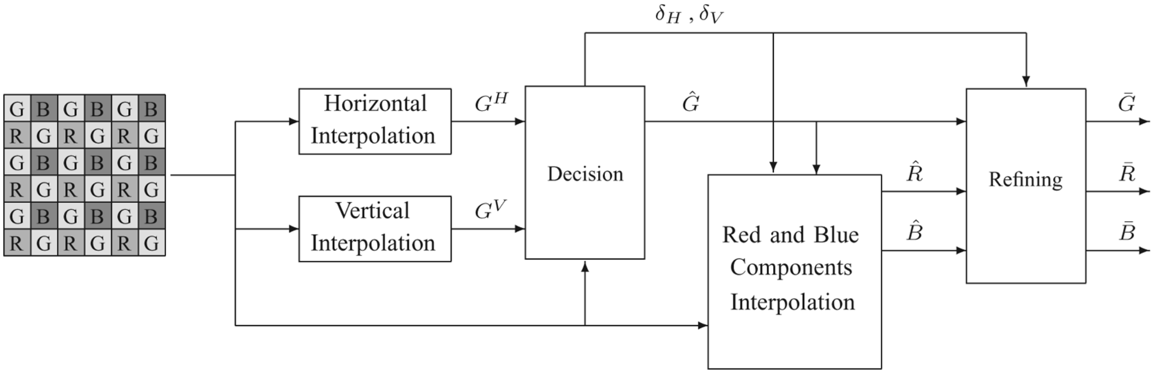

Fig. 2. Complete scheme of the proposed algorithm.

the CIELab color space. For each pixel the direction of interpolation that gives the most homogeneous neighborhood around the estimated pixel is chosen. In [20], instead, the decision is performed observing which directional reconstruction preserves the highest correlation of the color gradients, as usually found in natural images.

In this paper, we present a novel approach to demosaicing based on directional filtering and *a posteriori* decision, where the edge-directed interpolation is applied to reconstruct a full resolution green component, and then the red and blue channels are interpolated using the green information. Section II describes the proposed algorithm in detail. In Section III, an additional refining step to improve the quality of the reconstructed image is presented. The computational cost and the performance of the proposed approach are discussed in Section IV and compared to those of other recent demosaicing techniques. Finally, in Section V, we report the conclusions.

II. Proposed Algorithm

As seen in Section I and experimentally proved in [2], [19], and [20], some of the best demosaicing techniques are based on directional filtering. These algorithms initially compute two estimates f^H and f^V of the full color image. The green components G^H and G^V of these images are obtained through horizontal and vertical interpolation, respectively, and then the red and blue components are reconstructed using a bilinear interpolation of the color differences $R - G^H$ and $B - G^H$ for the horizontally estimated image f^H, and of $R - G^V$ and $B - G^V$ for the vertically estimated image f^V. Next, for each pixel, a choice between f^H and f^V is performed. This approach proved to give good performance; however, it requires us to compute and compare two full color images.

In this paper, we propose a more effective approach to directional interpolation, where the decision of the most suitable direction of interpolation is made on the basis of the reconstructed green component only. Once the choice is made, the red and blue components are interpolated. In this way, the two directional interpolations and the decision concern only one color component and not all the three channels. Moreover, this approach requires the decision only in a half of the pixels of the image, precisely where the sensor did not capture the green samples. Furthermore, since in this case the estimate of the green component after the decision is more accurate, a more efficient reconstruction of red and blue is possible.

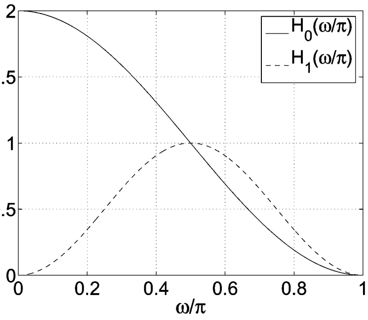

Fig. 3. Frequency response of the two filters h_0 and h_1.

Fig. 2 shows the complete scheme of the proposed demosaicing technique, and in the following we will describe its elements in detail.

A. Directional Green Interpolation

The first step of the algorithm is to reconstruct the green image along horizontal and vertical directions. To interpolate the Bayer samples, we apply a five-coefficient FIR filter. We do not use a longer filter because this would produce zipper effect near the edges. The filter we used is the same as [8], [19], and [20], and we rederived its coefficients on the basis of the following considerations.

We can note that, along a row (or a column) of the Bayer pattern, the green signal is subsampled with a factor of 2. In the frequency domain, this gives

$$G_s(\omega) = \frac{1}{2}G(\omega) + \frac{1}{2}G(\omega - \pi) \qquad (1)$$

where $G(\omega)$ and $G_s(\omega)$ denote the Fourier transform of the original green signal and of the down-sampled signal, respectively. Therefore, if $G(\omega)$ is band-limited to $|\omega| < \pi/2$, the ideal interpolation filter to perform the reconstruction would be

$$H_{id}(\omega) = 2\,\mathrm{rect}\left(\frac{\omega}{\pi}\right) \qquad (2)$$

since it eliminates the aliasing component $1/2G(\omega - \pi)$. The only FIR filter with three coefficients that we can apply to $G_s(\omega)$

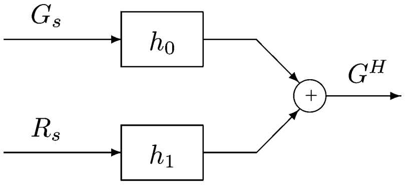

Fig. 4. Horizontal reconstruction of the green signal in a green-red row.

without modifying the average value of the samples is $h_0 = [0.5 \quad 1 \quad 0.5]$ (see Fig. 3).

However, this nonideal filter does not remove totally the aliasing. In fact, after filtering we have

$$\begin{aligned}\hat{G}(\omega) &= G_s(\omega)H_0(\omega)\\ &= \frac{1}{2}G(\omega)H_0(\omega) + \frac{1}{2}G(\omega-\pi)H_0(\omega)\end{aligned} \tag{3}$$

where the second term denotes the aliasing component.

A solution to decrease the aliasing effect and to improve the mid-frequency response could be to take advantage of the information coming from the high bands of the red and blue signals, since it is well known that the high frequencies of the color channels are highly correlated.

In a green-red row, the red component is sampled with an offset of one sample with respect to the green signal. Therefore, its Fourier transform results

$$R_s(\omega) = \frac{1}{2}R(\omega) - \frac{1}{2}R(\omega-\pi) \tag{4}$$

where $R(\omega)$ is the Fourier transform of the original red signal. If we interpolate it with a filter h_1 and we add the resulting signal to (3) as in Fig. 4, we have

$$\begin{aligned}\hat{G}(\omega) = \frac{1}{2}G(\omega)H_0(\omega) + \frac{1}{2}G(\omega-\pi)H_0(\omega) +\\ + \frac{1}{2}R(\omega)H_1(\omega) - \frac{1}{2}R(\omega-\pi)H_1(\omega).\end{aligned} \tag{5}$$

Reminding us that $R(\omega) - G(\omega)$ is slowly varying [8], [15], if h_1 is designed such that $H_1(\omega) \simeq 0$ at low frequencies and $H_1(\omega) \simeq H_0(\omega)$ at high frequencies, we have

$$R(\omega)H_1(\omega) \simeq G(\omega)H_1(\omega), \tag{6}$$

$$G(\omega-\pi)H_0(\omega) \simeq R(\omega-\pi)H_1(\omega) \tag{7}$$

and (5) could be approximated as

$$\hat{G}(\omega) \simeq \frac{1}{2}G(\omega)H_0(\omega) + \frac{1}{2}R(\omega)H_1(\omega). \tag{8}$$

A good choice for a filter h_1 that respects the constraints (6) and (7) is the five-coefficient FIR $[-0.25 \quad 0 \quad 0.5 \quad 0 \quad -0.25]$ (see Fig. 3).

Therefore, in the following row of the Bayer-sampled image:

$$\ldots \quad R_{-2} \quad G_{-1} \quad R_0 \quad G_1 \quad R_2 \quad \ldots$$

the missing green sample G_0 is estimated as

$$\hat{G}_0 = \frac{1}{2}(G_1 + G_{-1}) + \frac{1}{4}(2R_0 - R_2 - R_{-2}). \tag{9}$$

In [8], Adams follows a similar approach to derive this filter, while in [19], Hirakawa and Parks obtain the same filter starting from different constraints and solving an optimization problem to choose the filter's coefficients. An interesting interpretation of (9) is supplied by Wu and Zhang in [20], where they note that (9) can be written as

$$\hat{G}_0 = R_0 + \frac{1}{2}\left(G_1 - \frac{R_0 + R_2}{2} + G_{-1} - \frac{R_0 + R_{-2}}{2}\right). \tag{10}$$

That is, this reconstruction can also be considered as a bilinear interpolation of the $R-G$ difference, where the unknown values R_1 and R_{-1} are estimated as $(R_0 + R_2)/2$ and $(R_0 + R_{-2})/2$, respectively.

The interpolation of the green values in the blue-green rows and the interpolation along the columns follows the same approach.

B. Decision

Once the green component has been interpolated along both horizontal and vertical directions and two green images have been produced, a decision has to be made to select the filtering direction that gives the best performance.

As seen in the previous sections, a natural property of the images is the smoothness of the color differences. In fact, the color differences vary slowly and present abrupt changes only across the edges. Therefore, an image typically has greater values of the gradients of the color differences across the edges than along them. This property can be used to locate the presence and the direction of edges in a natural image and, hence, can be applied in the decision step to detect which is the most appropriate direction of interpolation, similarly to the procedure applied in [20].

Let G^H and G^V be the two interpolated green images. For each image, in every red or blue location (i.e., where the sensor acquired the red or blue values) we calculate the chrominance values $R - G^H$ (or $R - G^V$) in a red pixel, and $B - G^H$ (or $B - G^V$) in a blue pixel; namely

$$C_H(i,j) = \begin{cases} R_{i,j} - G^H_{i,j}, & \text{if} \quad (i,j) \quad \text{is a red location} \\ B_{i,j} - G^H_{i,j}, & \text{if} \quad (i,j) \quad \text{is a blue location} \end{cases}$$

$$C_V(i,j) = \begin{cases} R_{i,j} - G^V_{i,j}, & \text{if} \quad (i,j) \quad \text{is a red location} \\ B_{i,j} - G^V_{i,j}, & \text{if} \quad (i,j) \quad \text{is a blue location} \end{cases}$$

where i and j indicate the row and the column of the pixel (i,j), $1 \leq i \leq M$, $1 \leq j \leq N$ (M and N denote the height and the width of the image, respectively). Note that C_H and C_V are not defined in the green pixels. Next, we calculate the gradients of the chrominances and, precisely, the horizontal gradient for C_H and the vertical one for C_V

$$\begin{aligned} D_H(i,j) &= |C_H(i,j) - C_H(i,j+2)| \\ D_V(i,j) &= |C_V(i,j) - C_V(i+2,j)|. \end{aligned}$$

Note that, due to the structure of the Bayer pattern, the gradients are always computed as a difference of the same kind of chrominance ($R - G$ or $B - G$). For each red or blue pixel, we then define the classifiers $\delta_H(i,j)$ and $\delta_V(i,j)$ as the sum of the gradients D_H and D_V belonging to a sufficiently large

TABLE I
AVERAGE MSE FOR THE INTERPOLATION OF R IN THE GREEN AND BLUE LOCATIONS FOR THE FIVE TEST-IMAGES *LIGHTHOUSE*, *SAIL*, *BOAT*, *STATUE*, AND *WINDOW*

Locations	Bilinear Int. of $R - G$	Edge Directed [7]	Weighted Sum [10]	Proposed Algorithm
Green pixels	7.39	7.39	6.01	7.39
Blue pixels	17.03	17.52	16.88	13.39

TABLE II
MSE COMPARISON OF DIFFERENT TECHNIQUES FOR INTERPOLATING THE RED AND BLUE CHANNELS

Test-image		Bilinear	Edge Directed [7]	Weighted Sum [10]	Proposed Algorithm
lighthouse	R	10.92	11.20	9.90	**9.70**
	B	9.19	9.54	8.90	**7.68**
sail	R	5.70	5.73	**5.05**	5.22
	B	4.30	4.46	4.79	**3.66**
boat	R	11.06	11.43	10.16	**9.24**
	B	14.33	14.40	12.52	**12.15**
statue	R	6.90	6.90	**6.16**	6.23
	B	8.74	8.82	8.07	**7.77**
window	R	5.17	5.10	4.82	**4.81**
	B	6.59	6.48	**6.02**	6.13
Average	R	7.95	8.07	7.22	**7.04**
	B	8.63	8.74	8.45	**7.48**

neighborhood of (i, j) (for example, a 5 × 5 window gives good classifiers).

With a square window, both the classifiers are computed considering the same number of gradients based on the red chrominances and the same number of gradients based on the blue chrominances.

It this way, the two classifiers $\delta_H(i, j)$ and $\delta_V(i, j)$ give an estimate of the local variation of the color differences along the horizontal and vertical directions, respectively, and they can be used to estimate the direction of the edges. For example, if the value of δ_H is lower than δ_V, it is likely that there is a horizontal edge instead of a vertical one.

For all the red and blue pixels, we estimate the green values using the following criterion:

$$
\begin{aligned}
&\text{if} \quad \delta_V(i,j) < \delta_H(i,j)\\
&\text{then}\\
&\quad \hat{G}_{i,j} = G^V_{i,j};\\
&\text{else}\\
&\quad \hat{G}_{i,j} = G^H_{i,j}.
\end{aligned}
$$

So, considering also the known green samples, a full resolution green image $\hat{G}$ is estimated.

An additional improvement can be included in this procedure. Usually, in natural images, the majority of the edges and the details presents cardinal orientations. Therefore, if the pixel (i, j) is placed in a detailed area, during the estimation of the green values $\hat{G}_{i,j}$, it can result preferable to give more weight to the gradients D_H and D_V of the pixels in the same row and column of (i, j). This can be accomplished by weighting these gradients two or three times more than the other gradients when we calculate $\delta_H(i, j)$ and $\delta_V(i, j)$. In our implementation a weight of 3 is used to this purpose.

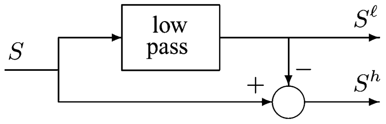

Fig. 5. Selection of the low-frequency and high-frequency components in the refining step ($S = R, G, B$).

C. Red and Blue Interpolation

After the green channel has been reconstructed, we have to interpolate the red and blue components. Besides the Bayer data, now we have a full resolution green image component $\hat{G}$ and the classifiers δ_H and δ_V that can be used for the reconstruction of the other two components.

In literature [4], [5], [7], [10], [11], [19]–[21], the most common approach for red and blue estimation consists in interpolation of the color differences $R - G$ and $B - G$, instead of R and B directly. Some particular reconstruction methods based upon the color differences have been explored,

TABLE III
MSE COMPARISON OF DIFFERENT APPROACHES FOR REFINING THE HIGH-FREQUENCY VALUES

Test-image		Before correction	After correction described in [22]	After proposed correction
lighthouse	R	9.70	8.14	8.21
	G	6.93	3.74	4.33
	B	7.68	5.84	6.03
sail	R	5.22	4.77	4.80
	G	3.17	2.07	2.16
	B	3.66	3.26	3.14
boat	R	9.24	6.77	6.90
	G	8.02	3.63	4.32
	B	12.15	9.94	9.89
statue	R	6.23	5.13	5.62
	G	5.17	2.77	3.33
	B	7.77	6.77	7.08
window	R	4.81	4.99	5.03
	G	3.29	2.38	2.50
	B	6.13	6.76	6.56
Average	R	7.04	5.96	6.11
	G	5.32	2.92	3.33
	B	7.48	6.51	6.54

such as the weighted sum proposed in [10], [11], and [21], or the Optimal Recovery, also explained in [21]. Nevertheless, the most used technique remains the bilinear interpolation, sometimes with a small modification for the reconstruction of red (or blue) component in the blue (red) pixels, where an edge-directed interpolation can be applied to interpolate the color differences along one of the two diagonal directions, selected with a laplacian operator [7].

Table I reports the average mean-square reconstruction error (MSE) for the red component of five test-images using different demosaicing approaches, in the green and the blue pixels, respectively. We note that, for all the approaches, the error is higher in the blue pixels then in the green ones. Similar results are found for the reconstruction of the blue channel.

For this reason, in the green locations we apply the bilinear interpolation of the color differences, as in other techniques, since it gives good performance with a low computational cost, while we propose a different approach to reconstruct the red values in the blue pixels and the blue values in the red ones.

Referring to the estimation of the red component (the same strategy is applied for the blue one), once all the green positions are interpolated, we use these estimated samples to reconstruct red also in the blue pixels. In fact, now each blue position has four estimated red neighbors placed in the cardinal directions. Therefore, we choose to perform an edge-directed interpolation using the estimated red samples in the green location. To decide the best direction we do not need a new edge-detection but we can use the classifiers δ_H and δ_V already applied in the reconstruction of the green component (remember that δ_H and δ_V have been computed for all the red and blue pixels). As opposed to other techniques, the cardinal directions are preferred with respect to the diagonal ones. This is justified by the fact that in natural images there are more cardinal edges with respect to the edges in other directions.

Moreover, notwithstanding it is well known that R and B are less correlated than R and G, we interpolate the color difference $R - B$ instead of $R - G$ because in the blue locations of the Bayer pattern it is found that interpolation using the difference $R - B$ gives an estimate of the red values more representative than using the difference $R - G$ (see Appendix 1 for details).

Therefore, in a blue position, the red is estimated as follows:

```
if $\delta_V(i,j) < \delta_H(i,j)$
then
    $\hat{R}_{i,j} = B_{i,j} + \frac{1}{2}\left(\hat{R}_{i-1,j} - \hat{B}_{i-1,j} + \hat{R}_{i+1,j} - \hat{B}_{i+1,j}\right)$
else
    $\hat{R}_{i,j} = B_{i,j} + \frac{1}{2}\left(\hat{R}_{i,j-1} - \hat{B}_{i,j-1} + \hat{R}_{i,j+1} - \hat{B}_{i,j+1}\right)$
```

For interpolation of the blue values in red pixels, the same strategy is applied.

In Table II, the performance of various techniques to reconstruct red and blue channels for several test images are reported (the green image has been interpolated following the approach explained in Sections II-A and II-B). Bilinear interpolation of the color differences, the edge-directed technique with estimation in the diagonal directions as in [7], the weighted sum of the color differences (using the weights proposed in [10]) and the proposed method are compared. Numbers in boldface indicate

TABLE IV
COMPUTATIONAL COST PER PIXEL OF DIFFERENT DEMOSAICING TECHNIQUES

	ADDSs	ABSs	SHIFTs	MULTSs	COMPs	LUTs	OPs
Bilinear Interpolation	4		3				7
Edge-Directed Interpolation [7]	16	4	4.5		1		25.5
Demosaicing with POCS [15]	400	4	4.5	384	1		793.5
Homogeneity-Directed Demosaicing [19]	106	12		50	103	6	277
Proposed Algorithm	19	1	4.5		1		25.5
Proposed Algorithm (with refining)	26.5	1	6	0.5	2		36

TABLE V
PSNR COMPARISON OF DIFFERENT DEMOSAICING METHODS (DECIBELS)

Method	Bilinear	[7]	[19]	[15]	[22]	Proposed
1	26.23	31.85	35.18	37.64	**38.36**	37.47
2	33.09	37.53	38.65	38.93	38.77	**40.15**
3	26.72	32.83	35.17	37.34	36.55	**37.45**
4	27.73	33.29	37.53	38.51	39.03	**39.64**
5	33.46	39.01	39.91	**41.47**	41.10	41.41
6	23.64	29.88	33.79	35.43	35.85	**35.87**
7	32.51	38.29	40.74	41.85	41.87	**42.41**
8	32.30	37.98	40.33	41.15	41.06	**42.17**
9	29.30	34.60	37.47	39.31	39.09	**39.58**
10	32.89	38.69	41.34	41.93	41.89	**43.01**
11	23.95	28.46	31.46	34.14	**34.96**	33.87
12	31.49	36.10	37.45	38.53	38.29	**38.93**
13	31.36	36.81	41.41	41.69	41.45	**43.36**
14	31.96	36.92	39.23	**40.85**	40.79	**40.85**
15	27.92	32.28	33.96	36.45	**36.74**	36.30
16	28.16	34.66	37.97	39.77	39.92	**40.07**
17	30.29	33.49	38.44	37.51	39.43	**39.97**
18	28.58	33.68	36.46	38.52	**39.06**	38.28
19	30.54	35.25	36.12	37.78	**37.95**	37.70
20	26.64	30.73	32.67	34.06	**34.64**	34.18
Ave.	29.44	34.62	37.26	38.64	38.84	**39.13**

the smallest values. Note that the proposed algorithm outperforms other methods in many images and its performance is at least comparable to that of more complex and computationally demanding approaches. Moreover, its complexity is as low as a simple bilinear interpolation.

III. REFINING STEP

The technique explained in Section II reconstructs in a fast way the full resolution image avoiding visible and annoying artifacts. However, even with an accurate selection of the edge directions, the reconstructed image may contain several errors due to the *interpolation artifacts* [19], less noticeable than misguidance artifacts (introduced by a wrong edge-estimation), but still annoying. In the proposed algorithm, they can be introduced by the approximations made in the filter design (see Section II-A) and, furthermore, by the low-pass characteristic of the filters used to interpolate the green component and the color differences $R-G$ and $B-G$. Note that these artifacts mainly affect the regions with high-frequency contents.

We propose to correct them by using the high bands interchannel correlation of the three primary colors. A good solution may consist in separating low- and high-frequency components in each pixel and replacing the high frequencies of the unknown components with the high frequencies of the Bayer-known component. The low-frequency component is preserved unchanged since the low-frequency components of the color channels are less correlated.

For example, for a green pixel in the location (i,j), the green value can be decomposed as

$$G_{i,j} = G^{\ell}_{i,j} + G^{h}_{i,j} \tag{11}$$

where G^{ℓ} and G^{h} denote the low- and high-frequency components, respectively, and the red and blue values can be corrected replacing R^h and B^h with G^h. That is

$$R_{i,j} = R^{\ell}_{i,j} + G^{h}_{i,j} \tag{12}$$

$$B_{i,j} = B^{\ell}_{i,j} + G^{h}_{i,j}. \tag{13}$$

The correction in the red and blue pixels is carried out in a similar way.

The selection of the low-frequency components is performed using a low-pass filter while the high frequencies are calculated subtracting the low-frequency values (see Fig. 5). The design of this low-pass filter is very important for the performance of the refining step and has to consider the following points.

A first important issue consists in exploiting the knowledge of the Bayer data, since we are sure that they are not affected by interpolation errors. So, it results preferable that the red (blue) component in the green locations, having only two neighbors belonging to the Bayer pattern, are corrected using a 1-D low-pass filter selecting only the red (blue) positions.

For the correction of the green channel and of the red and blue colors in the blue and red pixels, one possible choice is to span all the neighborhood, for example with a 2-D filter with a 3 × 3 kernel. A similar approach has been recently presented and analyzed in [22], where the color differences are filtered and successively used to correct the high frequencies of the image. However, an isotropic filtering may introduce zipper effect near the edges degrading the quality of the image since it performs the interpolation of the color differences also across the edges.

A more effective approach is to select the low and high frequencies using a 1-D filter, so the interpolation is carried out only along the edges of the image.

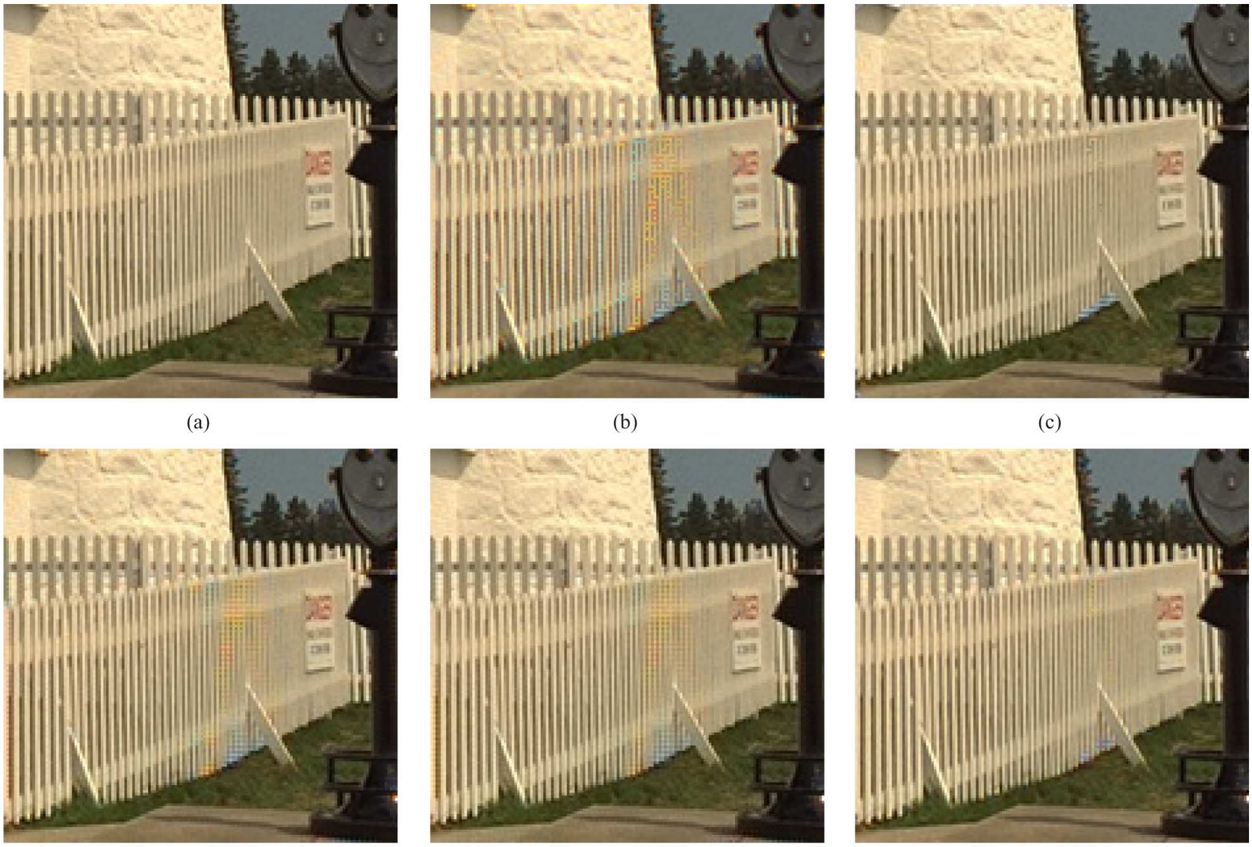

(a) (b) (c)

(d) (e) (f)

Fig. 6. Portion of the image *lighthouse*: (a) original image; (b) image reconstructed by technique [7]; (c) image reconstructed by technique [19]; (d) image reconstructed by technique [15]; (e) image reconstructed by technique [22]; (f) image reconstructed using the proposed algorithm. (Color version available online at http://ieeexplore.ieee.org.)

To summarize, the refining step is performed as follows.

1) **Updating of the green component**. For each red location (i, j), the green and red channels are filtered with a low-pass filter along the direction selected using δ_H and δ_V. The four components $G^{\ell}_{i,j}$, $G^{h}_{i,j}$, $R^{\ell}_{i,j}$, and $R^{h}_{i,j}$ are obtained. Then, the green high-frequency values $G^{h}_{i,j}$ are replaced with $R^{h}_{i,j}$ and the green samples $G_{i,j}$ are reconstructed. The same update is carried out for the green values in the blue locations.
2) **Updating of the red and blue components in the green locations.** For each green position, the green and the red subband values are obtained through horizontal or vertical filtering, depending on where the neighbor red values in the Bayer pattern are placed. Then, the high-frequency component of the red channel is updated with the green one and the red values are reconstructed. The update of the blue component is carried out in the same way.
3) **Updating of the red (blue) component in the blue (red) locations.** The red and blue channels are decomposed into low- and high-frequency components according to the most appropriate direction given by the comparison of δ_H and δ_V. The updated values in the neighboring pixels are used in order to obtain a more reliable estimate. Then, the red high-frequency component $R^{h}_{i,j}$ is replaced with $B^{h}_{i,j}$. The blue values in the red pixels are refined in a similar way.

Table III reports the MSE before and after the refining step for the test-images considered in Section II. The low-pass filter applied is the FIR $[1/3 \quad 1/3 \quad 1/3]$. We can notice that the updating improves the quality of the images, reducing the interpolation artifacts and the MSE values. The isotropic approach described in [22] (only one iteration) gives a bit smaller MSE values than the proposed method, but, on the other hand, a visual comparison of the interpolated images shows that the proposed technique avoids zippering near the edges and preserves with more precision the contours of the images (see Section IV).

IV. Computational Cost and Results

A. Computational Cost

An analysis of the computational complexity of the proposed approach can be done calculating all the operations required by the procedure described in the previous sections. The following operations are considered: additions, multiplications, absolute value computations, bit shifts and comparisons. The multiplications with powers of two are substituted with bit shifts.

Denoting with M and N the width and the height of the image, each directional interpolation of the green channel requires four additions and 3 bit shifts for half of the MN pixels of the image, while the decision step can be implemented with 18 additions, two absolute value computations, and one comparison for each one of the $\mathrm{MN}/2$ estimated values. So, the re-

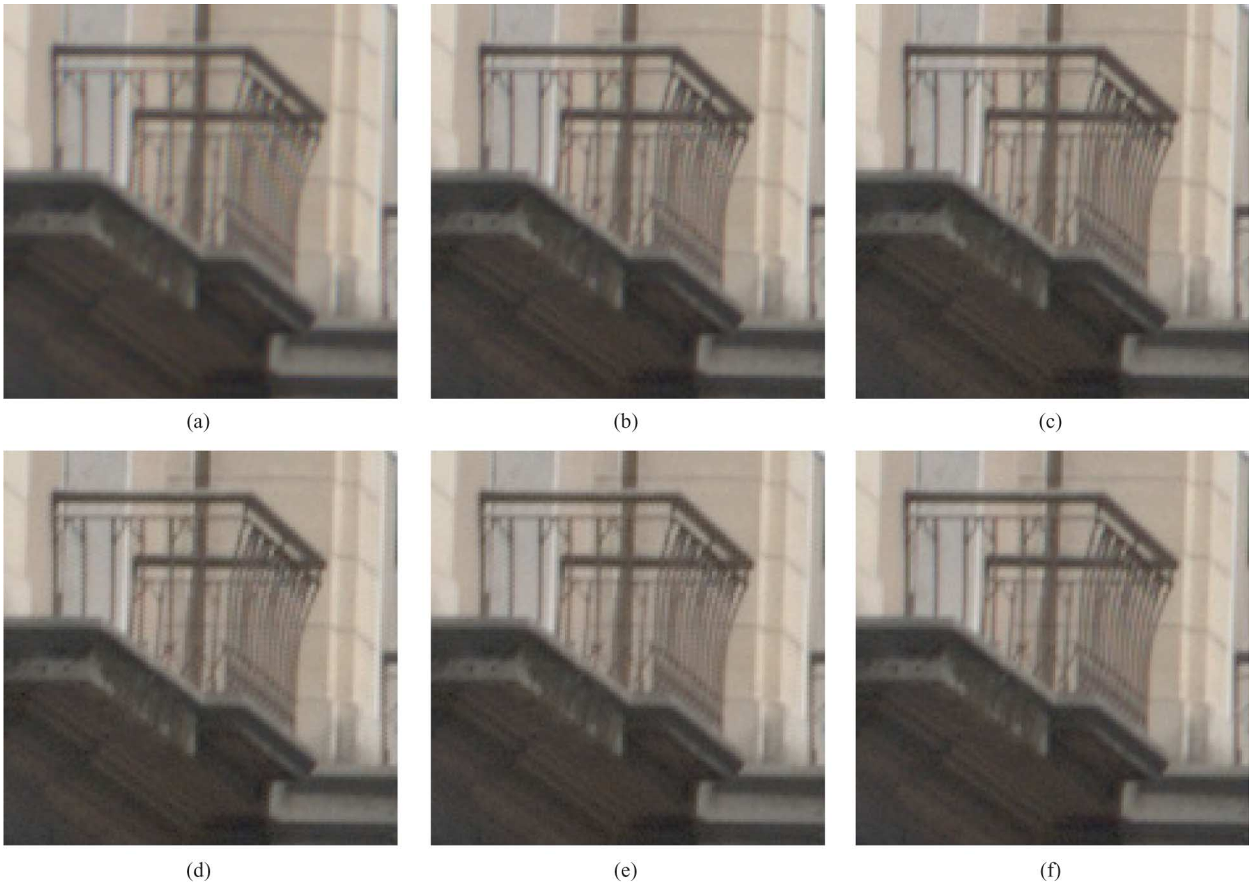

Fig. 7. Portion of an image captured with a Nikon D100 camera and demosaiced with the following methods: (a) bilinear interpolation; (b) technique [7]; (c) technique [19]; (d) technique [15]; (e) technique [22]; (f) proposed algorithm. (Color version available online at http://ieeexplore.ieee.org.)

construction of the green channels requires 13 MN additions, MN absolute value computations, 3 MN bit shifts, and 0.5 MN comparisons. Both the red and the blue interpolation need 3 MN additions, 0.75 MN bit shifts, and 0.25 MN comparisons. Therefore, producing a full color interpolated image requires 19 additions, one absolute value, 4.5 bit shifts, and one comparison per pixel.

The refining step described in Section III needs 7.5 additions, 1.5 bit shifts, 0.5 multiplication, and one comparison extra-operations per pixel. This step can be performed in real time when the computational resources of the camera allow the corresponding increase in complexity or as a postprocessing if the Bayer data are stored.

In Table IV, the computational cost of the proposed algorithm is compared with those of the demosaicing techniques described in [7], [15], [19]. The proposed scheme is very less demanding than other high-quality approaches (even including the additional refining step) and, as we shall see in Section IV-B, this is not paied with a reduction in performance.

B. *Experimental Results*

Table V reports the experimental results (in PSNR) of the proposed algorithm, using the set of 20 Kodak test images, used in [15]. These images are film captured and then digitized at the resolution of 512 × 768. We sampled them according to the Bayer pattern and afterwards we reconstructed them with different demosaicing techniques, comparing the interpolated images with the original ones. The algorithm described in Section II, with the refining step of Section III, is compared to the bilinear interpolation, the edge-directed approach of [7] and the recent demosaicing techniques presented in [15], [19], and [22]. For these three schemes, the MATLAB source code provided us by the authors was used.

The proposed algorithm outperforms the other techniques in the majority of the images and also the PSNR average is the highest. However, it is known that objective measures, such as MSE and PSNR, often fail to show the subjective quality of the images and a more effective evaluation is given by the visual inspection of the reconstructed images. In Fig. 6, a sample of the image *lighthouse* interpolated with different techniques is shown (this one and other images are available at the web site in [23]). It can be noticed that the proposed method presents less aliasing artifacts with respect to the other schemes. Moreover, because of the directional approach, also the zipper effect is avoided near the edges.

To give additional evidence of the performance of the proposed algorithm, we provide also some results obtained by demosaicing raw Bayer data captured using a Nikon D100 camera. This camera, which has a 6.1 megapixels CCD sensor with a Bayer color filter array, allows to store on its memory card the raw data in an uncompressed raw format.

TABLE VI
HIGH-FREQUENCY INTER-CHANNEL CORRELATION BETWEEN THE ORIGINAL RED SAMPLES AND THE ESTIMATED GREEN AND BLUE SAMPLES, RESPECTIVELY, IN THE BLUE LOCATIONS

	with 1-D filter		with 2-D filter	
	$\rho_{R\hat{B}}$	$\rho_{R\hat{G}}$	$\rho_{R\hat{B}}$	$\rho_{R\hat{G}}$
lighthouse	0.89	0.83	0.94	0.92
sail	0.86	0.80	0.92	0.90
boat	0.92	0.85	0.96	0.93
statue	0.88	0.84	0.92	0.88
window	0.88	0.85	0.92	0.90
Average	**0.89**	**0.83**	**0.93**	**0.91**

Fig. 7 shows a detail of one image demosaiced using the various techniques considered in this paper. The proposed algorithm and the most recent methods present little aliasing effects also in the high-frequency regions, but some algorithms introduce noticeable zipper effect along the edges of the image. It can be noticed that the proposed technique provides the best compromise between reconstruction of details and absence of zipper effect, also when compared to the most computational demanding methods. Again, this and few other images are available at the web site in [23].

V. CONCLUSION

In this paper, a novel approach to demosaicing based on directional filtering and *a posteriori* decision is presented. The experimental results confirms the effectiveness of this approach, providing excellent PSNR figures when compared to the most advanced demosaicing procedures, and avoiding visible artifacts such as aliasing and zippering. Moreover, the computational cost of the algorithm is kept low. Therefore, the proposed algorithm candidates itself for implementation in simple low-cost cameras or in video capture devices with high values of resolution and frame rate.

APPENDIX
ABOUT INTERCHANNEL CORRELATION

In natural images, it is a fact that red and blue components are less correlated than red and green or blue and green. For example, for the five test images used in Table II, we found an average correlation value of 0.84 between R and B, while the average correlations between G and R or B are 0.94 and 0.93, respectively. However, this fact is not indicative of which color difference ($R-B$ or $R-G$) is preferable to use to obtain the estimate of the red values in the blue pixels of the Bayer pattern, according to the method explained in Section II-C (the reconstruction of the blue in the red locations is totally symmetrical; hence, we refer only to the interpolation of R).

In fact, the formula applied for reconstructing a red sample in a blue location is

$$\hat{R}_i = C_i + \frac{1}{2}(\hat{R}_{i-1} - C_{i-1} + \hat{R}_{i+1} - C_{i+1}) \qquad (14)$$

where i denotes the horizontal or vertical coordinate, according to the direction of interpolation, and $C = \hat{G}$ if we interpolate the difference $R - G$, while $C = \hat{B}$ if we interpolate $R - B$. This equation can be rewritten as

$$\hat{R}_i = \frac{1}{2}(\hat{R}_{i-1} + \hat{R}_{i+1}) - \frac{1}{2}C_{i-1} + C_i - \frac{1}{2}C_{i+1} \qquad (15)$$

that is, the reconstruction of R consists in a bilinear interpolation of the two neighboring samples, corrected with the high-frequency content of the C component selected by the filter $[-0.5 \quad 1 \quad -0.5]$.

Therefore, for the correction, it is preferable to use the C color most correlated to the original red samples in the high frequencies. To select it, we calculate the high-frequency correlation coefficient in the blue locations of the Bayer pattern between the original red samples (that we have to estimate) and the available estimates of the green and blue components, namely $\rho_{R\hat{G}}$ and $\rho_{R\hat{B}}$. Two methods have been performed to compute the high frequencies, using two different high-pass filters. The first one has coefficients $[-0.5 \quad 1 \quad -0.5]$ and it is applied along the directions indicated by the edge-detection, as in Section II-C. The second is the 2-D high-pass filter

$$G = \begin{bmatrix} 0 & -0.25 & 0 \\ -0.25 & 1 & -0.25 \\ 0 & -0.25 & 0 \end{bmatrix}. \qquad (16)$$

The results are reported in Table VI. We see that, in the blue locations, the high frequencies of the estimated blue component are more correlated to the red values than to the high frequencies of the estimated green component. Therefore, the bilinear interpolation of $R - B$ gives a better approximation of the red samples than interpolation of $R - G$. This is not totally surprising, because, although the green channel is more accurately sampled in the Bayer pattern than the blue channel, here, we are referring to interpolation in the locations where the sensor captured the blue component.

ACKNOWLEDGMENT

The authors would like to thank B.K. Gunturk, K. Hirakawa, and X. Li for providing the software of their algorithms, and the anonymous reviewers for their comments which contribute to substantially improve the manuscript.

REFERENCES

[1] B. E. Bayer, "Color Imaging Array," U.S. Patent 3 971 065, 1976.

[2] B. K. Gunturk, J. Glotzbach, Y. Altunbasak, R. W. Schafer, and R. M. Mersereau, "Demosaicking: color filter array interpolation," *IEEE Signal Process. Mag.*, vol. 22, no. 1, pp. 44–54, Jan. 2005.

[3] D. R. Cok, "Signal Processing Method and Apparatus for Producing Interpolated Chrominance Values in a Sampled Color Image Signal," U.S. Patent 4 642 678, 1986.

[4] J. E. Adams, "Interactions between color plane interpolation and other image processing functions in electronic photography," *Proc. SPIE*, vol. 2416, pp. 144–151, Feb. 1995.

[5] C. A. Laroche and M. A. Prescott, "Apparatus and Method for Adaptively Interpolating a Full Color Image Utilizing Chrominance Gradients," U.S. Patent 5 373 322, 1994.

[6] R. H. Hibbard, "Apparatus and Method for Adaptively Interpolating a Full Color Image Utilizing Chrominance Gradients," U.S. Patent 5 382 976, 1995.

[7] J. F. Hamilton and J. E. Adams, "Adaptive Color Plane Interpolation in Single Sensor Color Electronic Camera," U.S. Patent 5 629 734, 1997.

[8] J. E. Adams, "Design of practical color filter array interpolation algorithms for digital cameras, part 2," in *Proc. IEEE Int. Conf. Image Processing*, Oct. 1998, vol. 1, pp. 488–492.

[9] R. Kakarala and Z. Baharav, "Adaptive demosaicing with the principal vector method," *IEEE Trans. Consum. Electron.*, vol. 48, no. 6, pp. 932–937, Nov. 2002.

[10] R. Kimmel, "Demosaicing: Image reconstruction from CCD samples," *IEEE Trans. Image Process.*, vol. 8, no. 9, pp. 1221–1228, Sep. 1999.

[11] W. Lu and Y.-P. Tan, "Color filter array demosaicing: New method and performance measures," *IEEE Trans. Image Process.*, vol. 12, no. 10, pp. 1194–1210, Oct. 2003.

[12] X. Wu, W. K. Choi, and P. Bao, "Color restoration from digital camera data by pattern matching," *Proc. SPIE*, vol. 3018, pp. 12–17, Apr. 1997.

[13] E. Chang, S. Cheung, and D. Pan, "Color filter array recovery using a threshold-based variable number of gradients," *Proc. SPIE*, vol. 3650, pp. 36–43, 1999.

[14] J. W. Glotzbach, R. W. Schafer, and K. Illgner, "A method of color filter array interpolation with alias cancellation properties," in *Proc. IEEE Int. Conf. Image Processing*, Oct. 2001, vol. 1, pp. 141–144.

[15] B. K. Gunturk, Y. Altunbasak, and R. M. Mersereau, "Color plane interpolation using alternating projections," *IEEE Trans. Image Process.*, vol. 11, no. 9, pp. 997–1013, Sep. 2002.

[16] D. H. Brainard, "Bayesian method for reconstructing color images from trichromatic samples," in *Proc. IS&T 47th Annu. Meeting*, 1994, pp. 375–380.

[17] D. Taubman, "Generalized wiener reconstruction of images from colour sensor data using a scale invariant prior," in *Proc. IEEE Int. Conf. Image Processing*, Sep. 2000, vol. 3, pp. 801–804.

[18] H. J. Trussell and R. E. Hartwig, "Mathematics for demosaicking," *IEEE Trans. Image Process.*, vol. 3, no. 4, pp. 485–492, Apr. 2002.

[19] K. Hirakawa and T. W. Parks, "Adaptive homogeneity-directed demosaicing algorithm," *IEEE Trans. Image Process.*, vol. 14, no. 3, pp. 360–369, Mar. 2005.

[20] X. Wu and N. Zhang, "Primary-consistent soft-decision color demosaicking for digital cameras (patent pending)," *IEEE Trans. Image Process.*, vol. 13, no. 9, pp. 1263–1274, Sep. 2004.

[21] D. D. Muresan and T. W. Parks, "Demosaicing using optimal recovery," *IEEE Trans. Image Process.*, vol. 14, no. 2, pp. 267–278, Feb. 2005.

[22] X. Li, "Demosaicing by successive approximation," *IEEE Trans. Image Process.*, vol. 14, no. 3, pp. 370–379, Mar. 2005.

[23] Demosaicing With Directional Filtering and a Posteriori Decision [Online]. Available: http://www.dei.unipd.it/ddfapd

Daniele Menon was born in 1979. He received the "Laurea in Ingegneria delle Telecomunicazioni" degree from the University of Padova, Padova, Italy, in 2004, where he is currently pursuing the Ph.D. degree.

During 2005, he was with the Department of Information Engineering at University of Padova, working in the European IST-MetaCamera project. His research interests concern image interpolation.

Stefano Andriani (S'05) received the "Laurea in Ingegneria delle Telecomunicazioni" degree from the University of Padova, Padova, Italy, in 2003.

Since then, he has been with the Department of Information Engineering, University of Padova, where he is currently pursuing the Ph.D. degree. His main research interests include lossless image and video compression, color image reconstruction, and hyperspectral image processing and coding. From 2003 to 2005, he was involved in the European IST-MetaCamera Project on Digital Cinema.

Giancarlo Calvagno (M'92) was born in Venezia, Italy, in 1962. He received the "Laurea in Ingegneria Elettronica" degree and the Doctorate degree in electrical engineering from the University of Padova, Padova, Italy, in 1986 and 1990, respectively.

From 1988 to 1990, he was with the Coordinated Science Laboratory of the University of Illinois at Urbana-Champaign, Urbana, as a Visiting Scholar. Since 1990, he has been with the Dipartimento di Ingegneria dell'Informazione, University of Padova, where he is currently an Associate Professor. His main research interests are in the areas of signal reconstruction, multidimensional signal processing, and image and video coding.